CHAPTER 5
Diffusion

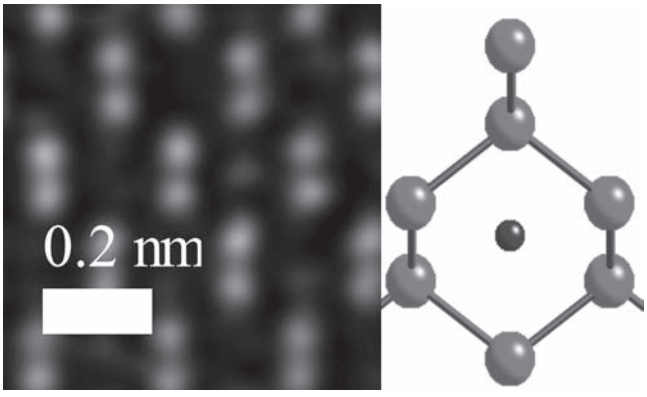

Atomic diffusion as introduced in this chapter involves individual atoms moving through crystal structures. In the high-resolution transmission electron micrograph on the left, we see a subtle image of one such atom in an interstitial position. The schematic illustration on the right shows this Ni atom to be in a silicon crystal as observed along the [110] *direction, the same orientation shown in the Chapter Opening micrograph in Chapter 3. (Courtesy of Klaus van Benthem and Andrew Thron, University of California, Davis.)*

During production and application, the chemical composition of engineering materials is often changed as a result of the movement of atoms, or *solid-state diffusion*. In some cases, atoms are redistributed within the microstructure of the material. In other cases, atoms are added from the material's environment, or atoms from the material may be discharged into the environment. Understanding the nature of the movement of atoms within the material can be critically important both in producing the material and in applying it successfully within an engineering design.

In Chapter 4, we were introduced to a variety of point defects, such as the vacancy. These defects were said to result typically from the thermal vibration of the atoms in the material. In this chapter, we will see the detailed relationship between temperature and the number of these defects. Specifically, the concentration of such defects rises exponentially with increasing temperature. The flow of atoms in engineering materials occurs by the movement of point defects, and, as a result, the rate of this solid-state diffusion increases exponentially with temperature. The mathematics of diffusion allows a precise description of the variation of the chemical composition within materials as a result of various diffusional processes. An important example is the *carburization* of steels, in which the surface is hardened by the diffusion of carbon atoms from a carbon-rich environment.

After some time, the chemical concentration profile within a material may become linear, and the corresponding mathematics for this *steady-state diffusion* is relatively simple.

Although we generally consider diffusion within the entire volume of a material, there are some cases in which the atomic transport occurs primarily along grain boundaries (by *grain boundary diffusion*) or along the surface of the material (by *surface diffusion*).

5.1 Thermally Activated Processes

A large number of processes in materials science and engineering share a common feature—the process rate rises exponentially with temperature. The diffusivity of elements in metal alloys, the rate of creep deformation in structural

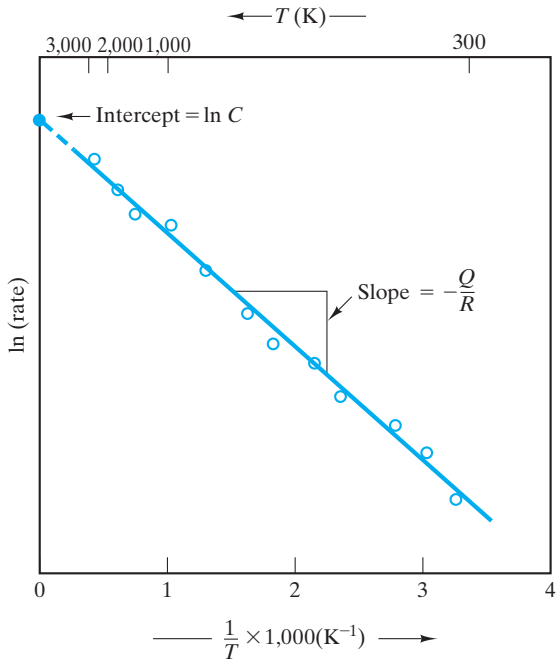

FIGURE 5.1 *Typical Arrhenius plot of data compared with Equation 5.2. The slope equals* $-Q/R$*, and the intercept* (at $1/T = 0$) *is ln C.*

materials, and the electrical conductivity of semiconductors are a few examples that will be covered in this book. The general equation that describes these various processes is of the form

$$\text{rate} = Ce^{-Q/RT}, \tag{5.1}$$

where C is a **preexponential constant** (independent of temperature), Q is the **activation energy**, R is the universal gas constant, and T is the absolute temperature. It should be noted that the universal gas constant is as important for the solid state as it is for the gaseous state. The term *gas constant* derives from its role in the perfect gas law ($pV = nRT$) and related gas-phase equations. In fact, R is a fundamental constant that appears frequently in this book devoted to the solid state.

Equation 5.1 is generally referred to as the **Arrhenius*** **equation**. Taking the logarithm of each side of Equation 5.1 gives

$$\ln (\text{rate}) = \ln C - \frac{Q}{R}\frac{1}{T}. \tag{5.2}$$

By making a semilog plot of ln (rate) versus the reciprocal of absolute temperature ($1/T$), one obtains a straight-line plot of rate data (Figure 5.1). The slope of the resulting **Arrhenius plot** is $-Q/R$. Extrapolation of the Arrhenius plot to $1/T = 0$ (or $T = \infty$) gives an intercept equal to ln C.

*Svante August Arrhenius (1859–1927), Swedish chemist, made numerous contributions to physical chemistry, including the experimental demonstration of Equation 5.1 for chemical reaction rates.

The experimental result of Figure 5.1 is a very powerful one. Knowing the magnitudes of process rate at any two temperatures allows the rate at a third temperature (in the linear-plot range) to be determined. Similarly, knowledge of a process rate at any temperature and of the activation energy, Q, allows the rate at any other temperature to be determined. A common use of the Arrhenius plot is to obtain a value of Q from measurement of the slope of the plot. This value of activation energy can indicate the mechanism of the process. In summary, Equation 5.2 contains two constants. Therefore, only two experimental observations are required to determine them.

To appreciate why rate data show the characteristic behavior of Figure 5.1, we must explore the concept of the activation energy, Q. As used in Equation 5.1, Q has units of energy per mole. It is possible to rewrite this equation by dividing both Q and R by Avogadro's number (N_{AV}), giving

$$\text{rate} = Ce^{-q/kT}, \tag{5.3}$$

where $q\ (= Q/N_{AV})$ is the activation energy per atomic scale unit (e.g., atom, electron, and ion) and $k\ (= R/N_{AV})$ is Boltzmann's* constant ($13.8 \times 10^{-24} J/K$). Equation 5.3 provides for an interesting comparison with the high-energy end of the **Maxwell–Boltzmann† distribution** of molecular energies in gases,

$$P \propto e^{-\Delta E/kT}, \tag{5.4}$$

where P is the probability of finding a molecule at an energy ΔE greater than the average energy characteristic of a particular temperature, T. Herein lies the clue to the nature of the activation energy. It is the energy barrier that must be overcome by **thermal activation**. Although Equation 5.4 was originally developed for gases, it applies to solids as well. As temperature increases, a larger number of atoms (or any other species involved in a given process, such as electrons or ions) is available to overcome a given energy barrier, q. Figure 5.2 shows a *process path* in which a single atom overcomes an energy barrier, q. Figure 5.3 shows a simple mechanical model of activation energy in which a box is moved from one position to another by going through an increase in potential energy, ΔE, analogous to the q in Figure 5.2.

In the many processes described in the text where an Arrhenius equation applies, particular values of activation energy will be found to be characteristic of process mechanisms. In each case, it is useful to remember that various possible mechanisms may be occurring simultaneously within the material, and each mechanism has a characteristic activation energy. The fact that one activation energy is representative of the experimental data means simply that a single mechanism is dominant. If the process involves several sequential steps,

---

*Ludwig Edward Boltzmann (1844–1906), Austrian physicist, is associated with many major scientific achievements of the 19th century (prior to the development of modern physics). The constant that bears his name plays a central role in the statistical statement of the second law of thermodynamics. Some ideas are difficult to put aside. His second law equation is carved on his tombstone.

†James Clerk Maxwell (1831–1879), Scottish mathematician and physicist, was an unusually brilliant and productive individual. His equations of electromagnetism are among the most elegant in all of science. He developed the kinetic theory of gases (including Equation 5.4) independently of his contemporary, Ludwig Edward Boltzmann.

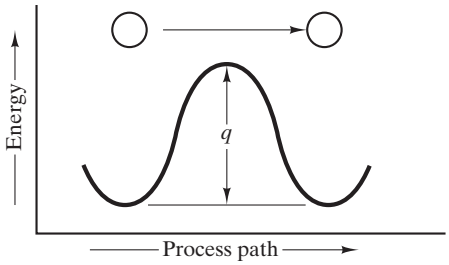

FIGURE 5.2 *Process path showing how an atom must overcome an activation energy, q, to move from one stable position to a similar adjacent position.*

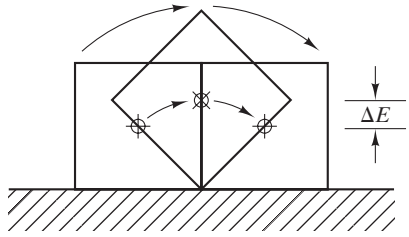

FIGURE 5.3 *Simple mechanical analog of the process path of Figure 5.2. The box must overcome an increase in potential energy, ΔE, in order to move from one stable position to another.*

the slowest step will be the **rate-limiting step**. The activation energy of the rate-limiting step, then, will be the activation energy for the overall process.

EXAMPLE 5.1

The rate at which a metal alloy oxidizes in an oxygen-containing atmosphere is a typical example of the practical utility of the Arrhenius equation (Equation 5.1). For example, the rate of oxidation of a magnesium alloy is represented by a rate constant, k. The value of k at 300°C is 1.05×10^{-8} kg/(m$^4 \cdot$ s). At 400°C, the value of k rises to 2.95×10^{-4} kg/(m$^4 \cdot$ s). Calculate the activation energy, Q, for this oxidation process (in units of kJ/mol).

SOLUTION

For this specific case, Equation 5.1 has the form

$$k = Ce^{-Q/RT}.$$

Taking the ratio of rate constants at 300°C (= 573 K) and 400°C (= 673 K), we conveniently cancel out the unknown preexponential constant, C, and obtain

$$\frac{2.95 \times 10^{-4}\text{kg}/[\text{m}^4 \cdot \text{s}]}{1.05 \times 10^{-8}\text{kg}/[\text{m}^4 \cdot \text{s}]} = \frac{e^{-Q/(8.314\ \text{J}/[\text{mol}\cdot\text{K}])(673\ \text{K})}}{e^{-Q/(8.314\ \text{J}/[\text{mol}\cdot\text{K}])(573\ \text{K})}}$$

or

$$2.81 \times 10^4 = e^{\{-Q/(8\,314\ \text{J}/[\text{mol}\cdot\text{K}])\}\{1/(673\ \text{K})-1/(573\ \text{K})\}},$$

giving

$$Q = 328 \times 10^3 \text{J/mol} = 328\ \text{kJ/mol}.$$

PRACTICE PROBLEM 5.1

Given the background provided by Example 5.1, calculate the value of the rate constant, k, for the oxidation of the magnesium alloy at 500°C.

5.2 Thermal Production of Point Defects

Point defects occur as a direct result of the periodic oscillation, or **thermal vibration**, of atoms in the crystal structure. As temperature increases, the intensity of this vibration increases and, thereby, the likelihood of structural disruption and the development of point defects increase. At a given temperature, the thermal energy of a given material is fixed, but this is an average value. The thermal energy of individual atoms varies over a wide range, as indicated by the Maxwell–Boltzmann distribution. At a given temperature, a certain fraction of the atoms in the solid have sufficient thermal energy to produce point defects. An important consequence of the Maxwell–Boltzmann distribution is that this fraction increases exponentially with absolute temperature. As a result, the concentration of point defects increases exponentially with temperature; that is,

$$\frac{n_{\text{defects}}}{n_{\text{sites}}} = Ce^{-(E_{\text{defect}})/kT}, \tag{5.5}$$

where $n_{\text{defects}}/n_{\text{sites}}$ is the ratio of point defects to ideal crystal-lattice sites, C is a preexponential constant, E_{defect} is the energy needed to create a single-point defect in the crystal structure, k is Boltzmann's constant, and T is the absolute temperature.

The temperature sensitivity of point-defect production depends on the type of defect being considered; that is, E_{defect} for producing a vacancy in a given crystal structure is different from E_{defect} for producing an interstitialcy.

Figure 5.4 illustrates the thermal production of vacancies in aluminum. The slight difference between the thermal expansion measured by overall sample dimensions ($\Delta L/L$) and by x-ray diffraction ($\Delta a/a$) is the result of vacancies. The x-ray value is based on unit-cell dimensions measured by x-ray diffraction (Section 3.7). The increasing concentration of empty lattice sites (vacancies) in the material at temperatures approaching the melting point produces a measurably greater thermal expansion as measured by overall dimensions. The concentration of vacancies (n_v/n_{sites}) follows the Arrhenius expression of Equation 5.5,

$$\frac{n_v}{n_{\text{sites}}} = Ce^{-E_V/kT}, \tag{5.6}$$

where C is a preexponential constant and E_V is the energy of formation of a single vacancy. As discussed previously, this expression leads to a convenient semilog plot of data. Taking the logarithm of each side of Equation 5.6 gives

$$\ln\frac{n_v}{n_{\text{sites}}} = \ln C - \frac{E_V}{k}\frac{1}{T}. \tag{5.7}$$

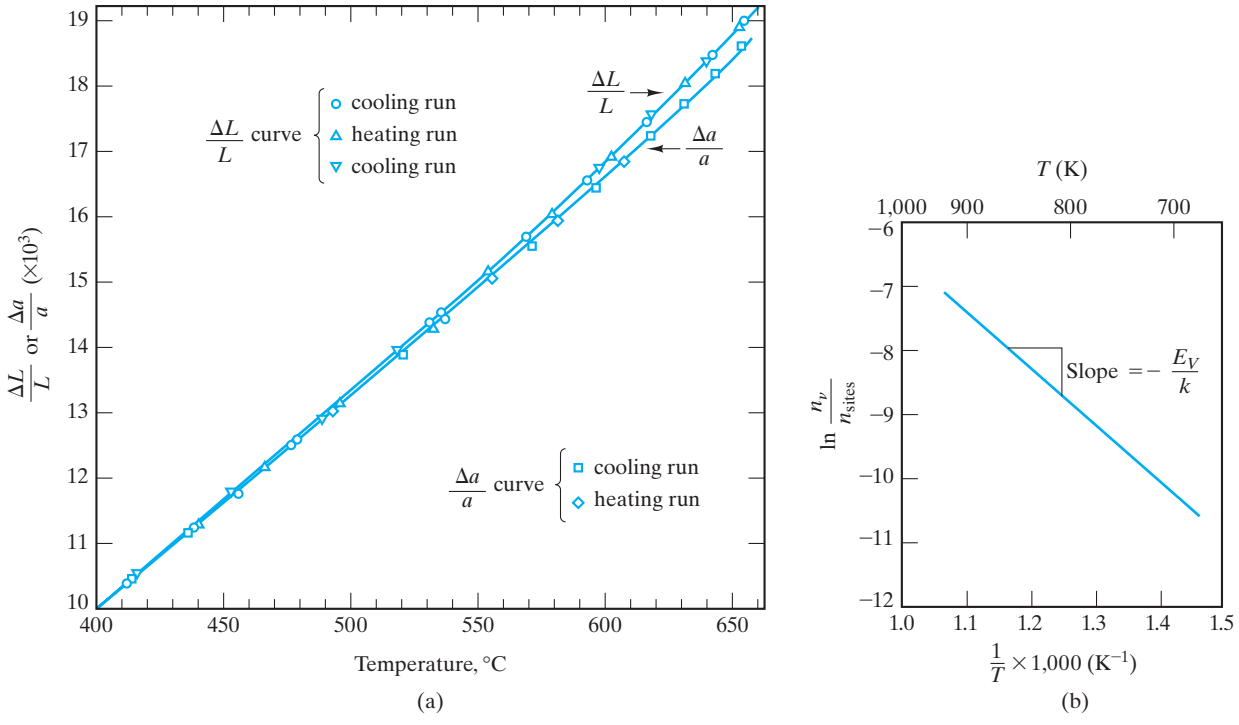

FIGURE 5.4 *(a) The overall thermal expansion* $(\Delta L/L)$ *of aluminum is measurably greater than the lattice parameter expansion* $(\Delta a/a)$ *at high temperatures because vacancies are produced by thermal agitation. (b) A semilog (Arrhenius-type) plot of ln (vacancy concentration) versus* $1/T$ *based on the data of part (a). The slope of the plot* $(-E_V/k)$ *indicates that* 0.76 *eV of energy is required to create a single vacancy in the aluminum crystal structure. (From P. G. Shewmon,* Diffusion in Solids, *McGraw-Hill Book Company, New York, 1963.)*

Figure 5.4 shows the linear plot of ln (n_v/n_{sites}) versus $1/T$. The slope of this Arrhenius plot is $-E_V/k$. These experimental data indicate that the energy required to create one vacancy in the aluminum crystal structure is 0.76 eV.

EXAMPLE 5.2

At 400°C, the fraction of aluminum lattice sites vacant is 2.29×10^{-5}. Calculate the fraction at 660°C (just below its melting point).

SOLUTION

From the text discussion relative to Figure 5.4, we have $E_V = 0.76$ eV. Using Equation 5.6, we have

$$\frac{n_v}{n_{\text{sites}}} = Ce^{-E_V/kT}.$$

At 400°C (= 673 K), we obtain

$$C = \left(\frac{n_v}{n_{\text{sites}}}\right) e^{+E_V/kT}$$

$$= (2.29 \times 10^{-5}) e^{+0.76\ \text{eV}/(86.2\times10^{-6}\text{eV/K})(673\ \text{K})} = 11.2.$$

At 660°C (= 933 K),

$$\frac{n_v}{n_{\text{sites}}} = (11.2) e^{-0.76\ \text{eV}/(86.2\times10^{-6}\text{eV/K})(933\ \text{K})} = 8.82 \times 10^{-4},$$

or roughly nine vacancies occur for every 10,000 lattice sites.

PRACTICE PROBLEM 5.2

Calculate the fraction of aluminum lattice sites vacant at **(a)** 500°C, **(b)** 200°C, and **(c)** room temperature (25°C). (See Example 5.2.)

5.3 Point Defects and Solid-State Diffusion

At sufficient temperatures, atoms and molecules can be quite mobile in both liquids and solids. Watching a drop of ink fall into a beaker of water and spread out until all the water is evenly colored gives a simple demonstration of **diffusion**, the movement of molecules from an area of higher concentration to an area of lower concentration. But diffusion is not restricted to different materials. At room temperature, H_2O molecules in pure water are in continuous motion and are migrating through the liquid as an example of **self-diffusion**. This atomic-scale motion is relatively rapid in liquids and relatively easy to visualize. It is more difficult to visualize diffusion in rigid solids. Nonetheless, diffusion does occur in the solid state. A primary difference between solid-state and liquid-state diffusion is the low rate of diffusion in solids. Looking back at the crystal structures of Chapter 3, we can appreciate that diffusion of atoms or ions through those generally tight structures is difficult. In fact, the energy requirements to squeeze most atoms or ions through perfect crystal structures are so high as to make diffusion nearly impossible. To make solid-state diffusion practical, point defects are generally required. Figure 5.5 illustrates how atomic migration becomes possible without major crystal-structure distortion by means of a **vacancy migration** mechanism. It is important to note that the overall direction of material flow is opposite to the direction of vacancy flow.

Figure 5.6 shows diffusion by an interstitialcy mechanism and illustrates effectively the **random-walk** nature of atomic migration. This randomness does not preclude the net flow of material when there is an overall variation in chemical composition. This frequently occurring case is illustrated in Figures 5.7 and 5.8. Although each atom of solid A has an equal probability of randomly "walking" in any direction, the higher initial concentration of A on the left side of the system will cause such random motion to produce *interdiffusion,* a net flow of A atoms into solid B. Similarly, solid B diffuses into solid A. The formal

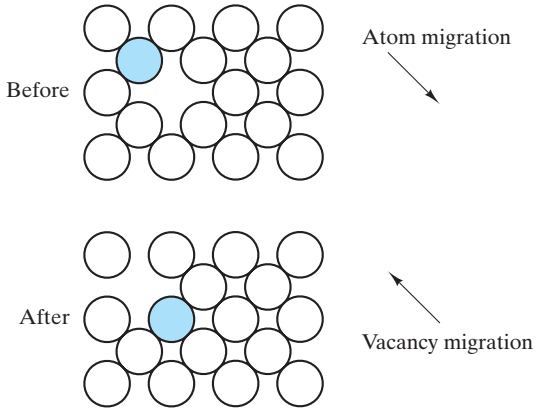

FIGURE 5.5 *Atomic migration occurs by a mechanism of vacancy migration. Note that the overall direction of material flow (the atom) is opposite to the direction of vacancy flow.*

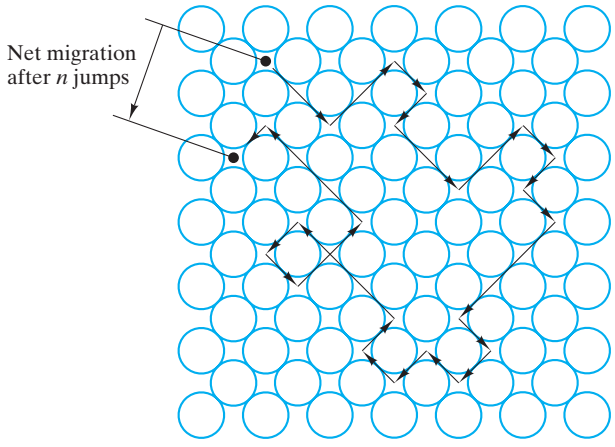

FIGURE 5.6 *Diffusion by an interstitialcy mechanism illustrating the random-walk nature of atomic migration.*

POWERS OF 10

The schematic illustrations on this page show how the atomic scale defects of Figure 4.8 facilitate diffusion. The application of these mechanisms in various heat treatments will be seen in Chapter 10.

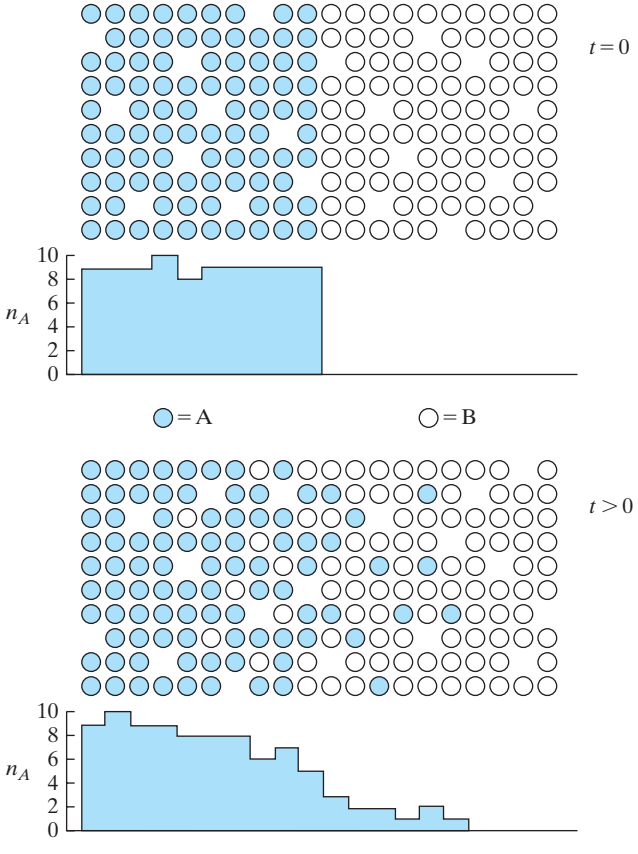

FIGURE 5.7 *The interdiffusion of materials* A *and* B. *Although any given* A *or* B *atom is equally likely to "walk" in any random direction (see Figure 5.6), the concentration gradients of the two materials can result in a net flow of* A *atoms into the* B *material, and vice versa.*

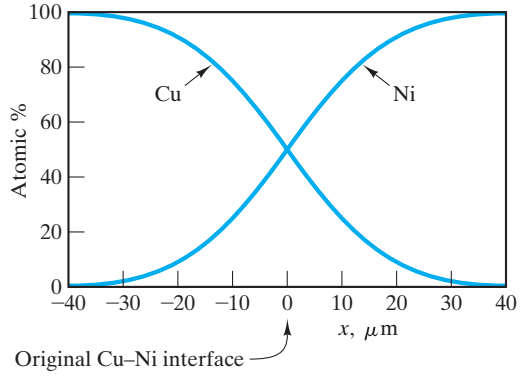

FIGURE 5.8 *The interdiffusion of materials on an atomic scale was illustrated in Figure 5.7. This interdiffusion of copper and nickel is a comparable example on the microscopic scale.*

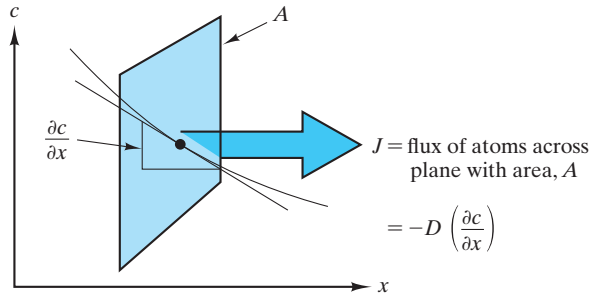

FIGURE 5.9 *Geometry of Fick's first law (Equation 5.8).*

mathematical treatment of such a diffusional flow begins with an expression known as **Fick's* first law**,

$$Jx = -D\frac{\partial c}{\partial x}, \tag{5.8}$$

where J_x is the *flux,* or flow rate, of the diffusing species in the x-direction due to a **concentration gradient** $(\partial c/\partial x)$. The proportionality coefficient, D, is called the **diffusion coefficient** or, simply, the **diffusivity**. The geometry of Equation 5.8 is illustrated in Figure 5.9. Figure 5.7 reminds us that the concentration gradient at a specific point along the diffusion path changes with time, t. This transient condition is represented by a second-order differential equation also known as **Fick's second law**,

$$\frac{\partial c_x}{\partial t} = \frac{\partial}{\partial x}\left(D\frac{\partial c_x}{\partial x}\right). \tag{5.9}$$

For many practical problems, one can assume that D is independent of c, leading to a simplified version of Equation 5.9:

$$\frac{\partial c_x}{\partial t} = D\frac{\partial^2 c_x}{\partial x^2}. \tag{5.10}$$

Figure 5.10 illustrates a common application of Equation 5.10, the diffusion of material into a semi-infinite solid while the surface concentration of the diffusing species, c_s, remains constant. Two examples of this system would be the plating of metals and the saturation of materials with reactive atmospheric gases. Specifically, steel surfaces are often hardened by **carburization**, the diffusion of carbon atoms into the steel from a carbon-rich environment. The solution to this differential equation with the given boundary conditions is

$$\frac{c_x - c_0}{c_s - c_0} = 1 - \text{erf}\left(\frac{x}{2\sqrt{Dt}}\right), \tag{5.11}$$

---

*Adolf Eugen Fick (1829–1901), German physiologist. The medical sciences frequently apply principles previously developed in the fields of mathematics, physics, and chemistry. However, Fick's work in the "mechanistic" school of physiology was so excellent that it served as a guide for the physical sciences. He developed the diffusion laws as part of a study of blood flow.

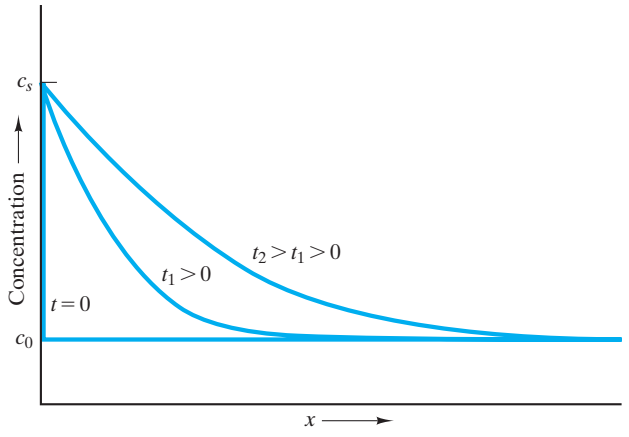

FIGURE 5.10 *Solution to Fick's second law (Equation 5.10) for the case of a semi-infinite solid, constant surface concentration of the diffusing species c_s, initial bulk concentration c_0, and a constant diffusion coefficient, D.*

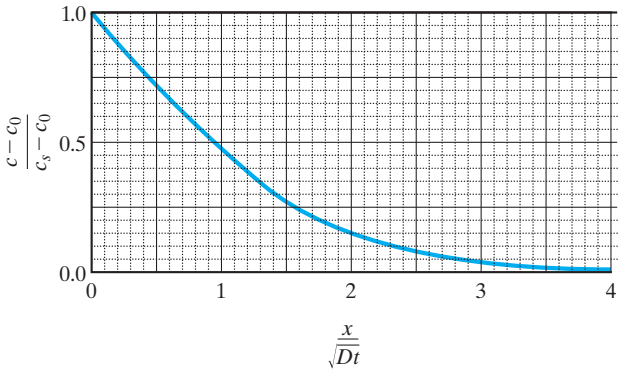

FIGURE 5.11 *Master plot summarizing all of the diffusion results of Figure 5.10 on a single curve.*

where c_0 is the initial bulk concentration of the diffusing species and erf refers to the **Gaussian* error function**, based on the integration of the "bell-shaped" curve with values readily available in mathematical tables. Representative values are given in Table 5.1. A great power of this analysis is that the result (Equation 5.11) allows all of the concentration profiles of Figure 5.10 to be redrawn on a single master plot (Figure 5.11). Such a plot permits rapid calculation of the time necessary for relative saturation of the solid as a function of x, D, and t.

The preceding mathematical analysis of diffusion implicitly assumed a fixed temperature. Our previous discussion of the dependence of diffusion on point defects causes us to expect a strong temperature dependence for diffusivity by analogy to Equation 5.5—and this is precisely the case. Diffusivity data are perhaps the best known examples of an Arrhenius equation

$$D = D_0 e^{-q/kT}, \tag{5.12}$$

where D_0 is the preexponential constant and q is the activation energy for defect motion. In general, q is not equal to the E_{defect} of Equation 5.5. E_{defect} represents the energy required for defect formation, while q represents the energy required for the movement of that defect through the crystal structure ($E_{\text{defect motion}}$) for *interstitial diffusion.* For the vacancy mechanism, vacancy formation is an integral part of the diffusional process (see Figure 5.5), and $q = E_{\text{defect}} + E_{\text{defect motion}}$.

*Johann Karl Friedrich Gauss (1777–1855), German mathematician, was one of the great geniuses in the history of mathematics. In his teens, he developed the method of least squares for curve-fitting data. Much of his work in mathematics was similarly applied to physical problems, such as astronomy and geomagnetism. His contribution to the study of magnetism led to the unit of magnetic-flux density being named in his honor.

TABLE 5.1

The Error Function

z	erf(z)	z	erf(z)
0.00	0.0000	0.70	0.6778
0.01	0.0113	0.75	0.7112
0.02	0.0226	0.80	0.7421
0.03	0.0338	0.85	0.7707
0.04	0.0451	0.90	0.7969
0.05	0.0564	0.95	0.8209
0.10	0.1125	1.00	0.8427
0.15	0.1680	1.10	0.8802
0.20	0.2227	1.20	0.9103
0.25	0.2763	1.30	0.9340
0.30	0.3286	1.40	0.9523
0.35	0.3794	1.50	0.9661
0.40	0.4284	1.60	0.9763
0.45	0.4755	1.70	0.9838
0.50	0.5205	1.80	0.9891
0.55	0.5633	1.90	0.9928
0.60	0.6039	2.00	0.9953
0.65	0.6420		

Source: Handbook of Mathematical Functions, M. Abramowitz and I. A. Stegun, Eds., National Bureau of Standards, Applied Mathematics Series 55, Washington, DC, 1972.

It is more common to tabulate diffusivity data in terms of molar quantities (i.e., with an activation energy, Q, per mole of diffusing species),

$$D = D_0 e^{-Q/RT}, \tag{5.13}$$

where R is the universal gas constant ($= N_{AV}k$,) as discussed previously. Figure 5.12 shows an Arrhenius plot of the diffusivity of carbon in α-Fe over a range of temperatures, which is an example of an interstitialcy mechanism as sketched in Figure 5.6. Figure 5.13 collects diffusivity data for a number of metallic systems. Table 5.2 gives the Arrhenius parameters for these data. It is useful to compare different data sets. For instance, C can diffuse by an interstitialcy mechanism through bcc Fe more readily than through fcc Fe ($Q_{bcc} < Q_{fcc}$ in Table 5.2). The greater openness of the bcc structure (Section 3.2) makes this difference understandable. Similarly, the self-diffusion of Fe by a vacancy mechanism is greater in bcc Fe than in fcc Fe. Figure 5.14 and Table 5.3 give comparable diffusivity data for several nonmetallic systems. In many compounds, such as Al_2O_3, the smaller ionic species (e.g., Al^{3+}) diffuse much more readily through the system. The Arrhenius behavior of ionic diffusion in ceramic compounds is especially analogous to the temperature dependence of semiconductors to be discussed in Chapter 13. It is this ionic transport mechanism that is responsible for the semiconducting behavior of certain ceramics such as ZnO; that is, charged ions rather than electrons produce the measured electrical conductivity. Polymer data are not included with the other nonmetallic systems of Figure 5.14 and Table 5.3 because most commercially important diffusion mechanisms in polymers involve the liquid state or the amorphous solid state, where the point-defect mechanisms of this section do not apply.

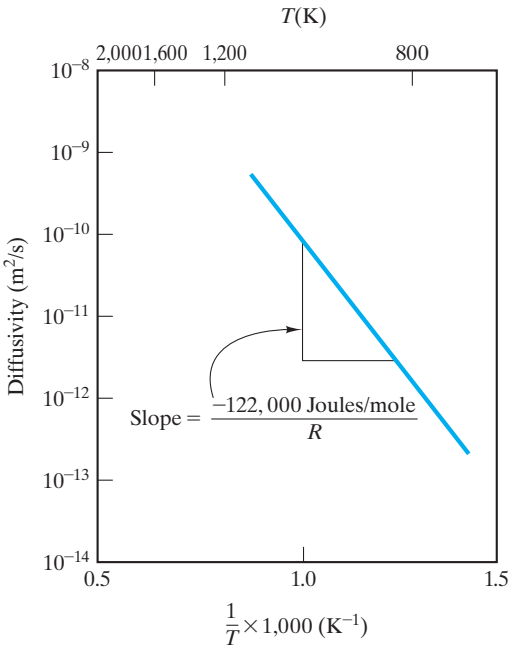

FIGURE 5.12 *Arrhenius plot of the diffusivity of carbon in α-iron over a range of temperatures. Note also related Figures 4.4 and 5.6 and other metallic diffusion data in Figure 5.13.*

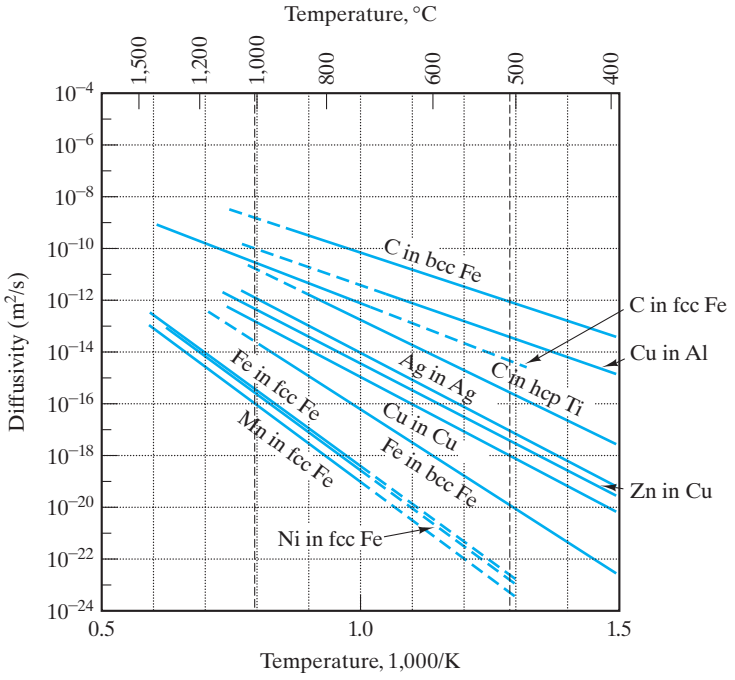

FIGURE 5.13 *Arrhenius plot of diffusivity data for a number of metallic systems. (From L. H. Van Vlack,* Elements of Materials Science and Engineering, *4th ed., Addison-Wesley Publishing Co., Inc., Reading, MA, 1980.)*

TABLE 5.2

Diffusivity Data for a Number of Metallic Systems[a]

Solute	Solvent	D_0(m²/s)	Q(kJ/mol)	Q(kcal/mol)
Carbon	Fcc iron	20×10^{-6}	142	34.0
Carbon	Bcc iron	220×10^{-6}	122	29.3
Iron	Fcc iron	22×10^{-6}	268	64.0
Iron	Bcc iron	200×10^{-6}	240	57.5
Nickel	Fcc iron	77×10^{-6}	280	67.0
Manganese	Fcc iron	35×10^{-6}	282	67.5
Zinc	Copper	34×10^{-6}	191	45.6
Copper	Aluminum	15×10^{-6}	126	30.2
Copper	Copper	20×10^{-6}	197	47.1
Silver	Silver	40×10^{-6}	184	44.1
Carbon	Hcp titanium	511×10^{-6}	182	43.5

[a]See Equation 5.13.

Source: Data from L. H. Van Vlack, *Elements of Materials Science and Engineering*, 4th ed., Addison-Wesley Publishing Co., Inc., Reading, MA, 1980.

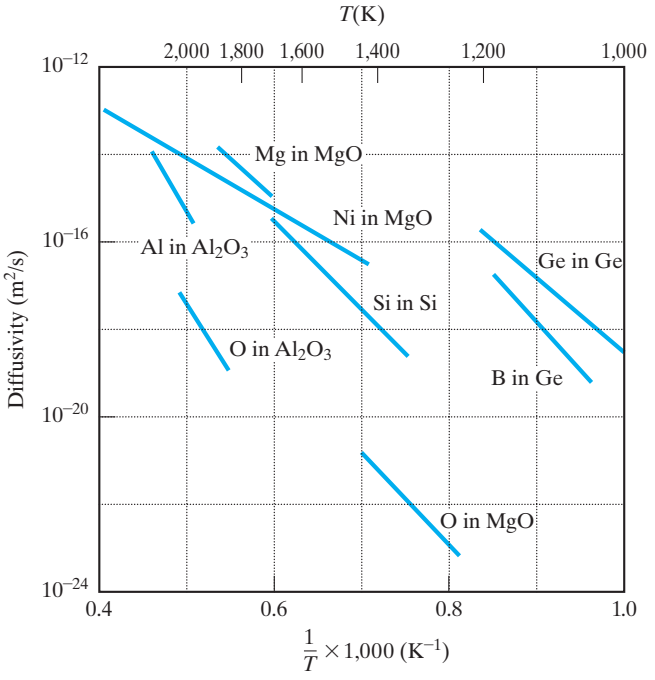

FIGURE 5.14 *Arrhenius plot of diffusivity data for a number of nonmetallic systems. (From P. Kofstad,* Nonstoichiometry, Diffusion, and Electrical Conductivity in Binary Metal Oxides, *John Wiley & Sons, Inc., NY, 1972; and S. M. Hu in* Atomic Diffusion in Semiconductors, *D. Shaw, Ed., Plenum Press, New York, 1973.)*

TABLE 5.3

Diffusivity Data for a Number of Nonmetallic Systems[a]

Solute	Solvent	D_0(m²/s)	Q(kJ/mol)	Q(kcal/mol)
Al	Al_2O_3	2.8×10^{-3}	477	114.0
O	Al_2O_3	0.19	636	152.0
Mg	MgO	24.9×10^{-6}	330	79.0
O	MgO	4.3×10^{-9}	344	82.1
Ni	MgO	1.8×10^{-9}	202	48.3
Si	Si	0.18	460	110.0
Ge	Ge	1.08×10^{-3}	291	69.6
B	Ge	1.1×10^{3}	439	105.0

[a]See Equation 5.13.

Source: Data from P. Kofstad, *Nonstoichiometry, Diffusion, and Electrical Conductivity in Binary Metal Oxides,* John Wiley & Sons, Inc., New York, 1972; and S. M. Hu, in *Atomic Diffusion in Semiconductors,* D. Shaw, Ed., Plenum Press, New York, 1973.

EXAMPLE 5.3

Steel surfaces can be hardened by *carburization,* as discussed relative to Figure 5.10. During one such treatment at 1,000°C, there is a drop in carbon concentration from 5 to 4 at % carbon between 1 and 2 mm from the surface of the steel. Estimate the flux of carbon atoms into the steel in this near-surface region. (The density of γ-Fe at 1,000°C is 7.63 g/cm^3.)

SOLUTION

First, we approximate

$$\frac{\partial c}{\partial x} \simeq \frac{\Delta c}{\Delta x} = \frac{5 \text{ at } \% - 4 \text{ at } \%}{1 \text{ mm} - 2 \text{ mm}}$$
$$= -1 \text{ at } \%/\text{mm}.$$

To obtain an absolute value for carbon-atom concentration, we must first know the concentration of iron atoms. From the given data and Appendix 1,

$$\rho = 7.63 \frac{g}{\text{cm}^3} \times \frac{0.6023 \times 10^{24} \text{atoms}}{55.85 \text{ g}} = 8.23 \times 10^{22} \frac{\text{atoms}}{\text{cm}^3}.$$

Therefore,

$$\frac{\Delta c}{\Delta x} = -\frac{0.01(8.23 \times 10^{22} \text{atoms/cm}^3)}{1 \text{ mm}} \times \frac{10^6 \text{cm}^3}{\text{m}^3} \times \frac{10^3 \text{mm}}{\text{m}}$$

$$= -8.23 \times 10^{29} \text{atoms/m}^4.$$

From Table 5.2,

$$D_c \text{ in } \gamma - \text{Fe}, 1000°\text{C} = D_0 e^{-Q/RT}$$
$$= (20 \times 10^{-6} \text{m}^2/\text{s}) e^{-(142{,}000 \text{ J/mol})/(8.314 \text{ J/mol/K})(1273 \text{ K})}$$
$$= 2.98 \times 10^{-11} \text{m}^2/\text{s}.$$

Using Equation 5.8 gives us

$$J_x = -D\frac{\partial c}{\partial x}$$
$$\simeq -D\frac{\Delta c}{\Delta x}$$
$$= -(2.98 \times 10^{-11} \text{m}^2/\text{s})(-8.23 \times 10^{29} \text{atoms/m}^4)$$
$$= 2.45 \times 10^{19} \text{atoms/(m}^2 \cdot \text{s)}$$

EXAMPLE 5.4

The diffusion result described by Equation 5.11 can apply to the carburization process (Example 5.3). The carbon environment (a hydrocarbon gas) is used to set the surface-carbon content (c_s) at 1.0 wt %. The initial carbon content of the steel (c_0) is 0.2 wt %. Using the error-function table, calculate how long it would take at 1,000°C to reach a carbon content of 0.6 wt % [i.e., $(c - c_0)/(c_s - c_0) = 0.5$] at a distance of 1 mm from the surface.

SOLUTION

Using Equation 5.11, we get

$$\frac{c_x - c_0}{c_s - c_0} = 0.5 = 1 - \text{erf}\left(\frac{x}{2\sqrt{Dt}}\right)$$

or

$$\text{erf}\left(\frac{x}{2\sqrt{Dt}}\right) = 1 - 0.5 = 0.5.$$

Interpolating from Table 5.1 gives

$$\frac{0.5 - 0.4755}{0.5205 - 0.4755} = \frac{z - 0.45}{0.50 - 0.45}$$

or

$$z = \frac{x}{2\sqrt{Dt}} = 0.4772$$

or

$$t = \frac{x^2}{4(0.4772)^2 D}.$$

Using the diffusivity calculation from Example 5.3, we obtain

$$\begin{aligned} t &= \frac{(1 \times 10^{-3}\text{m})^2}{4(0.4772)^2(2.98 \times 10^{-11}\text{m}^2/\text{s})} \\ &= 3.68 \times 10^4\,\text{s} \times \frac{1\,\text{h}}{3.6 \times 10^3\,\text{s}} \\ &= 10.2\,\text{h}. \end{aligned}$$

EXAMPLE 5.5

Recalculate the carburization time for the conditions of Example 5.4 using the master plot of Figure 5.11 rather than the error-function table.

SOLUTION

From Figure 5.11, we see that the condition for $(c - c_0)/(c_S - c_0) = 0.5$ is

$$\frac{x}{\sqrt{Dt}} \simeq 0.95$$

or

$$t = \frac{x^2}{(0.95)^2 D}.$$

Using the diffusivity calculation from Example 5.3, we obtain

$$t = \frac{(1 \times 10^{-3}\text{m})^2}{(0.95)^2(2.98 \times 10^{-11}\text{m}^2/\text{s})}$$

$$= 3.72 \times 10^4\text{s} \times \frac{1\text{ h}}{3.6 \times 10^3\text{s}}$$

$$= 10.3\text{ h}.$$

Note. There is appropriately close agreement with the calculation of Example 5.4. Exact agreement is hindered by the need for graphical interpretation (in this problem) and tabular interpolation (in the previous problem).

EXAMPLE 5.6

For a carburization process similar to that in Example 5.5, a carbon content of 0.6 wt % is reached at 0.75 mm from the surface after 10 h. What is the carburization temperature? (Assume, as before, that $c_s = 1.0$ wt % and $c_0 = 0.2$ wt %.)

SOLUTION

As in Example 5.5,

$$\frac{x}{\sqrt{Dt}} \simeq 0.95$$

or

$$D = \frac{x^2}{(0.95)^2 t}$$

with the following data given:

$$D = \frac{(0.75 \times 10^{-3}\text{m})^2}{(0.95)^2(3.6 \times 10^4\text{s})} = 1.73 \times 10^{-11}\text{m}^2/\text{s}.$$

From Table 5.2, for C in γ-Fe,

$$D = (20 \times 10^{-6}\text{m}^2/\text{s})e^{-(142{,}000\ \text{J/mol})/[8.314\ \text{J/(mol}\cdot K)](T)}$$

Equating the two values for D gives

$$1.73 \times 10^{-11}\frac{\text{m}^2}{\text{s}} = 20 \times 10^{-6}\frac{\text{m}^2}{\text{s}}e^{-1.71\times10^4/T}$$

or

$$T^{-1} = \frac{-\ln\,(1.73 \times 10^{-11}/20 \times 10^{-6})}{1.71 \times 10^4}$$

or

$$T = 1225\ \text{K} = 952°\text{C}.$$

PRACTICE PROBLEM 5.3

Suppose that the carbon-concentration gradient described in Example 5.3 occurred at 1,100°C rather than at 1,000°C. Calculate the carbon-atom flux for this case.

PRACTICE PROBLEM 5.4

In Example 5.4, the time to generate a given carbon concentration profile is calculated using the error-function table. The carbon content at the surface was 1.0 wt % and at 1 mm from the surface was 0.6 wt %. For this diffusion time, what is the carbon content at a distance **(a)** 0.5 mm from the surface and **(b)** 2 mm from the surface?

PRACTICE PROBLEM 5.5

Repeat Practice Problem 5.4 using the graphical method of Example 5.5.

PRACTICE PROBLEM 5.6

In Example 5.6, a carburization temperature is calculated for a given carbon-concentration profile. Calculate the carburization temperature if the given profile were obtained in 8 hours rather than 10 hours, as originally stated.

5.4 Steady-State Diffusion

The change in the concentration profile with time for processes such as carburization was shown in Figure 5.10. A similar observation for a process with slightly different boundary conditions is shown in Figure 5.15. In this case, the relatively high surface concentration of the diffusing species, c_h, is held constant with time, just as c_s was held constant in Figure 5.10, but the relatively low concentration, c_l,

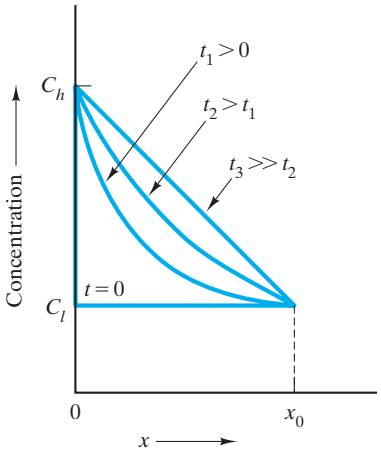

FIGURE 5.15 *Solution to Fick's second law (Equation 5.10) for the case of a solid of thickness x_0, constant surface concentrations of the diffusing species c_h and c_l, and a constant diffusion coefficient D. For long times (e.g., t_3), the linear concentration profile is an example of steady-state diffusion.*

at x_0 is also held constant with time. As a result, the nonlinear concentration profiles at times greater than zero (e.g., at t_1 and t_2 in Figure 5.15) approach a straight line after a relatively long time (e.g., at t_3 in Figure 5.15). This *linear* concentration profile is unchanging with additional time as long as c_h and c_l remain fixed. This limiting case is an example of **steady-state diffusion** (i.e., mass transport that is unchanging with time). The concentration gradient defined by Equation 5.8 takes an especially simple form in this case:

$$\frac{\partial c}{\partial x} = \frac{\Delta c}{\Delta x} = \frac{c_h - c_l}{0 - x_0} = -\frac{c_h - c_l}{x_0}. \tag{5.14}$$

In the case of carburization represented by Figure 5.10, the surface concentration, c_s, was held fixed by maintaining a fixed carbon-source atmospheric pressure at the $x = 0$ surface. In this same way, both c_h and c_l are maintained fixed in the case represented by Figure 5.15. A plate of material with a thickness of x_0 is held between two gas atmospheres: a high-pressure atmosphere on the $x = 0$ surface, which produces the fixed concentration c_h, and a low-pressure atmosphere on the $x = x_0$ surface, which produces the concentration c_l (Figure 5.16).

A common application of steady-state diffusion is the use of materials as gas purification membranes. For example, a thin sheet of palladium metal is permeable to hydrogen gas, but not to common atmospheric gases such as oxygen, nitrogen, and water vapor. By introducing the "impure" gas mixture on the high-pressure side of Figure 5.16b and maintaining a constant, reduced hydrogen pressure on the low-pressure side, a steady flow of purified hydrogen passes through the palladium sheet.

EXAMPLE 5.7

A 5-mm-thick sheet of palladium with a cross-sectional area of 0.2 m^2 is used as a steady-state diffusional membrane for purifying hydrogen. If the hydrogen concentration on the high-pressure (impure gas) side of the sheet is 0.3 kg/m^3 and the diffusion coefficient for hydrogen in Pd is $1.0 \times 10^{-8} m^2/s$, calculate the mass of hydrogen being purified per hour.

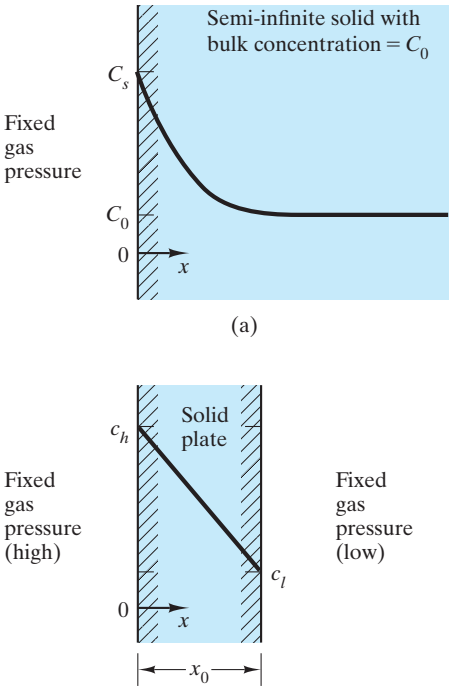

FIGURE 5.16 *Schematic of sample configurations in gas environments that lead, after a long time, to the diffusion profiles representative of (a) nonsteady state diffusion (Figure 5.10) and (b) steady-state diffusion (Figure 5.15).*

SOLUTION

Fick's first law (Equation 5.8) is simplified by the steady-state concentration gradient of Equation 5.14, giving

$$\begin{aligned} Jx &= -D(\partial c/\partial x) = -D[-(c_h - c_l)/x_0] \\ &= -(1.0 \times 10^{-8}\text{m}^2/\text{s})[-(0.3\ \text{kg/m}^3 - 0\ \text{kg/m}^3)/(5 \times 10^{-3}\ \text{m})] \\ &= 0.6 \times 10^{-6}\text{kg/m}^2 \cdot \text{s} \times 3.6 \times 10^3\text{s/h} = 2.16 \times 10^{-3}\ \text{kg/m}^2 \cdot \text{h} \end{aligned}$$

The total mass of hydrogen being purified will then be this flux times the membrane area:

$$m = Jx \times A = 2.16 \times 10^{-3}\text{kg/m}^2 \cdot \text{h} \times 0.2\ \text{m}^2 = 0.432 \times 10^{-3}\text{kg/h}.$$

PRACTICE PROBLEM 5.7

For the purification membrane in Example 5.7, how much hydrogen would be purified per hour if the membrane used is 3 mm thick, with all other conditions unchanged?

THE MATERIAL WORLD

Diffusion in Fuel Cells

William Grove, an English jurist and amateur physicist, discovered the principle of the fuel cell in 1839. Grove used four large cells, each containing hydrogen and oxygen, to produce electric power that was then used to split water in another cell into hydrogen and oxygen gases. In 1842, he wrote to the great English chemist and physicist Michael Faraday: "I cannot but regard the experiment as an important one." Grove's confidence was appropriate, but somewhat premature.

More than a century passed until, in 1959, NASA demonstrated the potential of fuel cells to provide power during space flight. This demonstration stimulated industry to explore applications in the 1960s, but technical barriers and high investment costs prevented commercialization. In 1984, the Office of Transportation Technologies at the U.S. Department of Energy began supporting research and development in fuel-cell technology. Today, hundreds of companies worldwide, including several major automakers, are vigorously pursuing fuel-cell technology.

Diffusion plays a key role in modern fuel-cell designs. As the accompanying figure shows, a fuel cell is an electrochemical energy conversion device. (A major attraction is that it is between two and three times more efficient than an internal combustion engine in converting fuel to power.) As hydrogen flows into the fuel cell on the anode side, the hydrogen gas is separated into hydrogen ions (protons) and electrons at the surface of a platinum catalyst. The hydrogen ions diffuse across the membrane and combine with oxygen and electrons at the surface of another platinum catalyst on the cathode side (producing water, the only emission from a hydrogen fuel cell!).

The electrons cannot pass through the nonconductive membrane and, instead, produce a current from the anode to the cathode via an external circuit that provides about enough power for a single lightbulb. By stacking enough cells in series, sufficient power to run automobiles and other large-scale systems is possible.

Substantial research is under way on optimizing the membrane material. Both polymeric and ceramic materials are under investigation. Related research involves fuels other than pure hydrogen and the infrastructure required to deliver these fuels on a wide scale. Ironically, another diffusion problem (the transport of water out of the fuel cell) is one of the technological challenges to commercialization. Nonetheless, the significant potential of fuel-cell technology is quite promising, more than 160 years after William Grove's "important" experiment, and governments and private industry are together investing billions of dollars in these efforts.

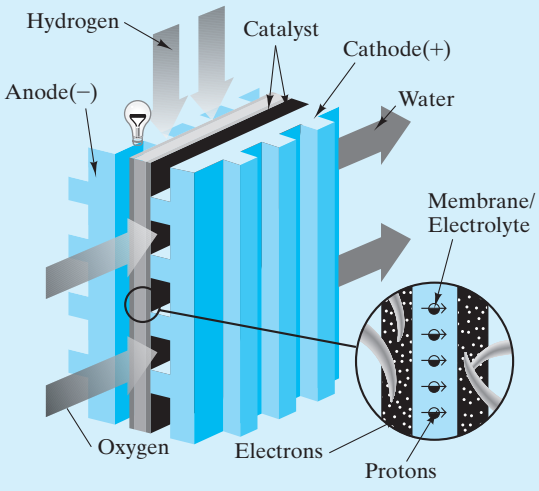

(From *Fuel Cells–Green Power,* Los Alamos National Laboratory Report LA-UR-99-3231.)

Prototype fuel-cell-powered Toyota sport utility vehicle evaluated at the University of California, Davis. (Courtesy of the University of California, Davis.)

5.5 Alternate Diffusion Paths

A final word of caution is in order about using specific diffusivity data to analyze a particular material process. Figure 5.17 shows that the self-diffusion coefficients for silver vary by several orders of magnitude, depending on the route for diffusional transport. To this point, we have considered **volume diffusion**, or **bulk diffusion**, through a material's crystal structure by means of some defect mechanism. However, there can be "short circuits" associated with easier diffusion paths. As seen in Figure 5.17, diffusion is much faster (with a lower Q) along a grain boundary. As we saw in Section 4.4, this region of mismatch between adjacent crystal grains in the material's microstructure is a more open structure, allowing enhanced grain-boundary diffusion. The crystal surface is an even more open region, and **surface diffusion** allows easier atom transport along the free surface less hindered by adjacent atoms. The overall result is that

$$Q_{\text{volume}} > Q_{\text{grain boundary}} > Q_{\text{surface}} \text{ and } D_{\text{volume}} < D_{\text{grain boundary}} < D_{\text{surface}}.$$

This result does not mean that surface diffusion is always the important process just because D_{surface} is greatest. More important is the amount of diffusing region available. In most cases, volume diffusion dominates. For a material with a small average grain size (see Section 4.4) and therefore a large grain-boundary area, **grain-boundary diffusion** can dominate. Similarly, in a fine-grained powder with a large surface area, surface diffusion can dominate.

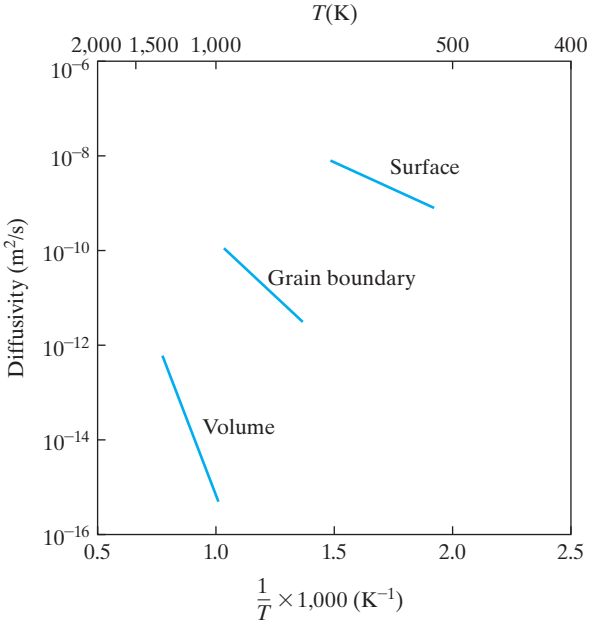

FIGURE 5.17 *Self-diffusion coefficients for silver depend on the diffusion path. In general, diffusivity is greater through less-restrictive structural regions.*

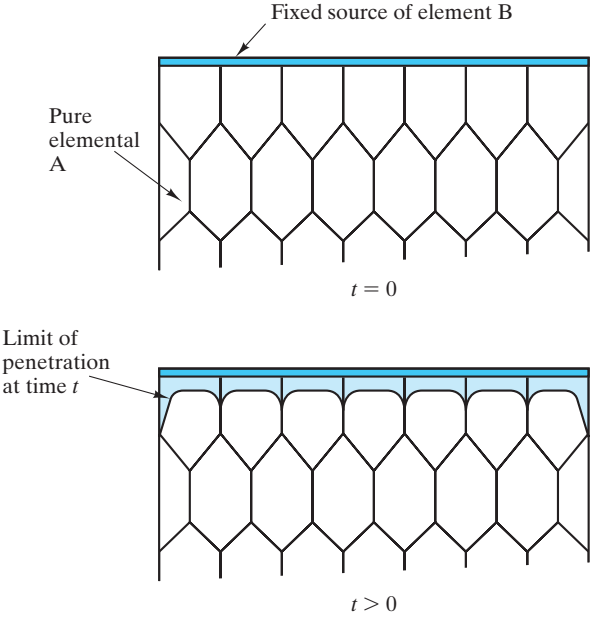

FIGURE 5.18 *Schematic illustration of how a coating of impurity* B *can penetrate more deeply into grain boundaries and even further along a free surface of polycrystalline* A, *consistent with the relative values of diffusion coefficients* ($D_{\text{volume}} < D_{\text{grain boundary}} < D_{\text{surface}}$).

For a given polycrystalline microstructure, the penetration of a diffusing species will tend to be greater along grain boundaries and even greater along the free surface of the sample (Figure 5.18).

EXAMPLE 5.8

We can approximate the extent of grain-boundary penetration in Figure 5.18 by using the semi-infinite diffusion expression of Equation 5.11. **(a)** Taking $D_{\text{grain boundary}} = 1.0 \times 10^{-10}\,\text{m}^2/\text{s}$, calculate the penetration of B into A along the grain boundary after 1 hour, defined as the distance, x, at which $c_x = 0.01c_s$ (with $c_0 = 0$ for initially pure A). **(b)** For comparison, calculate the penetration defined in the same way within the bulk grain for which $D_{\text{volume}} = 1.0 \times 10^{-14}\,\text{m}^2/\text{s}$.

SOLUTION

(a) We can simplify Equation 5.11 as

$$\frac{c_x - c_0}{c_s - c_0} = 1 - \text{erf}\left(\frac{x}{2\sqrt{Dt}}\right) = \frac{c_x - 0}{c_s - 0} = \frac{0.01c_s}{c_s} = 0.01,$$

or

$$\text{erf}\left(\frac{x}{2\sqrt{Dt}}\right) = 1 - 0.01 = 0.99.$$

Interpolating from Table 5.1 gives

$$\frac{0.9928 - 0.99}{0.9928 - 0.9891} = \frac{1.90 - z}{1.90 - 1.80},$$

or

$$z = \frac{x}{2\sqrt{Dt}} = 1.824,$$

and then

$$x = 2(1.824)\sqrt{Dt}$$

$$= 2(1.824)\sqrt{(1.0 \times 10^{-10}\,\text{m}^2/\text{s})(1\,\text{h})(3.6 \times 10^3\,\text{s/h})}$$

$$= 2.19 \times 10^{-3}\,\text{m} = 2.19\,\text{mm}.$$

(b) For comparison,

$$x = 2(1.824)\sqrt{(1.0 \times 10^{-14}\,\text{m}^2/\text{s})(1\,\text{h})(3.6 \times 10^3\,\text{s/h})}$$

$$= 21.9 \times 10^{-6}\,\text{m} = 21.9\,\mu\text{m}.$$

Note. The amount of grain-boundary penetration calculated in **(a)** is exaggerated, as the excess buildup of impurity, B, in the boundary leads to some of that material being "drained away" by side diffusion into the A grains, as indicated by Figure 5.18.

PRACTICE PROBLEM 5.8

In Example 5.8, we calculated the extent of impurity penetration for volume and grain-boundary paths. For further comparison, calculate the penetration for surface diffusion for which $D_{surface} = 1.0 \times 10^{-8}\,m^2/s$.

Summary

The point defects introduced in Chapter 4 are seen to play a central role in the movement of atoms by solid-state diffusion. Several practical problems in the production and application of engineering materials involve these diffusional processes.

Specifically, we find that point-defect concentrations increase exponentially with absolute temperature following an Arrhenius expression. As solid-state diffusion in crystalline materials occurs via a point-defect mechanism, the diffusivity, as defined by Fick's laws, also increases exponentially with absolute temperature in another Arrhenius expression.

The mathematics of diffusion allows a relatively precise description of the chemical concentration profiles of diffusing species. For some sample geometries, the concentration profile approaches a simple, linear form after a relatively long time. This steady-state diffusion is well illustrated by gas transport across thin membranes.

In the case of fine-grained polycrystalline materials or powders, material transport may be dominated by grain-boundary diffusion or surface diffusion, respectively, because, in general, $D_{volume} < D_{grain\ boundary} < D_{surface}$. Another result is that, for a given polycrystalline solid, impurity penetration will be greater along grain boundaries and even greater along the free surface.

Key Terms

activation energy (127)
Arrhenius equation (127)
Arrhenius plot (127)
bulk diffusion (146)
carburization (134)
concentration gradient (134)
diffusion (132)
diffusion coefficient (134)
diffusivity (134)
Fick's first law (134)
Fick's second law (134)
Gaussian error function (135)
grain-boundary diffusion (146)
Maxwell–Boltzmann distribution (128)
preexponential constant (127)
random-walk (132)
rate-limiting step (129)
self-diffusion (132)
steady-state diffusion (143)
surface diffusion (146)
thermal activation (128)
thermal vibration (130)
vacancy migration (132)
volume diffusion (146)